Application of scanning thermal microscopy for thermal conductivity measurements on meso-porous silicon thin films

2007 J. Phys. D: Appl. Phys. 40 6677

(http://iopscience.iop.org/0022-3727/40/21/029)

IOP Publishing Journal of Physics D: Applied Physics
J. Phys. D: Appl. Phys. **40** (2007) 6677–6683 doi:10.1088/0022-3727/40/21/029

Application of scanning thermal microscopy for thermal conductivity measurements on meso-porous silicon thin films

S Gomès[1], L David[1], V Lysenko[2], A Descamps[1], T Nychyporuk[2] and M Raynaud[1]

[1] Centre de Thermique de Lyon, UMR CNRS 5008, Institut National des Sciences Appliquées de Lyon, Université Claude Bernard Lyon 1, Domaine Scientifique de la Doua, INSA-Lyon, Bâtiment Sadi Carnot, 9, rue de la Physique, F-69621, Villeurbanne Cedex, France
[2] Institut des Nanotechnologies de Lyon, UMR CNRS 5270, INSA de Lyon, Domaine Scientifique de la Doua, INSA-Lyon, Bâtiment Blaise Pascal, 7, avenue Jean Capelle, F-69621, Villeurbanne cedex, France

E-mail: severine.gomes@insa-lyon.fr and vladimir.lysenko@insa-lyon.fr

Received 4 July 2007, in final form 7 September 2007
Published 19 October 2007
Online at stacks.iop.org/JPhysD/40/6677

Abstract
A scanning thermal microscope (SThM) in the dc regime was used to study the thermal conductivity of homogeneous in-depth meso-porous silicon in the form of thin films on a monocrystalline silicon substrate. Measurements for different film porosities (30–80%) and thicknesses (100 nm–8 μm) were performed in order to estimate the influence of both layer porosity and thickness on the thermal conductivity values of porous silicon (PS). An analytical model predicting the SThM measurement in the case of ultra-thin monolayered samples was used to calibrate the technique, to analyse experimental data and to determine the thermal conductivity of meso-porous layers. Effective thermal conductivity of meso-PS films was found to decrease when the porosity increases. The effective thermal conductivities measured for thick porous layers (several μm) are in good accordance with those measured by micro-Raman-spectroscopy on bulk meso-PS samples. For submicrometric thicknesses (<1 μm), the effective thermal conductivity of layers decreases significantly with decreasing layer thickness due to the increased sensitivity of measurements to the thermal resistance of the film/substrate interface. An intrinsic thermal conductivity of PS was calculated independently of the film thickness and the values of interfacial thermal resistances were thus estimated. From the apparatus point of view, the results obtained show that the depth being sensed is of the order of a few micrometres for insulating materials and depends on the thermal conductivity of the films.

1. Introduction

Thermal conductivity measurements on thin nanostructured porous dielectric films have attracted considerable attention over the last decade. The main reason for this is the development of thin film device applications in microelectronics and microtechnologies. Nanostructured porous low-k materials permit improvements, for example, through the decrease in RC (resistance $\times$ capacitance) delay of the integrated device functioning. However, if line-to-line capacitance and cross-talk noise in the interconnections can be reduced, power dissipation in these low-density porous

materials is still a problematic issue [1]. The study of thermal conductivity of the thin nanostructured low-k films therefore plays a crucial role. Considering meso-porous silicon (meso-PS) as one of such nanomaterials, we have studied its thermal conductivity with the use of scanning thermal microscopy (SThM). Meso-PS nanostructures have already been reported to be used as a thermal insulating material for fabrication of thermal sensors [2] or integrated devices [3]. For this purpose, thick ($>10\,\mu$m) meso-PS layers were mainly considered. Thermal conductivity values of the thick porous layers were published to be about two or three orders of magnitude lower than thermal conductivity of the monocrystalline silicon ($147\,\mathrm{W\,m^{-1}\,K^{-1}}$) [4–11]. However, what is the thermal conductivity of thinner meso-PS films? These data will be especially important if one wants to integrate the thin meso-PS films into a chip structure.

In recent years many methods have been developed for the thermal conductivity measurement of thin films. Such measurements were performed on various materials: insulators (SiO_2 film on a Si substrate [12], ZrO_2 on Al_2O_3 [13], etc), semiconductors (doped single-crystalline Si films [14], superlattice materials [15], etc) and metals (Al films on Si and Cu substrates [16], Ni film on a quartz substrate [17]). The following measurement methods can be mentioned, for example: electrical resistance variations in strips deposited on the surface of a studied sample when it is electrically (3ω method) [18] or optically [19] heated, changes in the optical properties of surfaces such as the reflection coefficient in a modulated thermo-reflectance technique [20, 21]. Furthermore, the surface temperature can be measured using a modulated photothermal infrared radiometry technique [22]. For most of the studied film/substrate pairs, the film thermal conductivity decreases with a reduction of the film thickness because of the influence of the film/substrate interface introducing an additional thermal resistance and acting as a boundary scattering place for thermal energy carriers. This decrease also takes place when the film thickness overlaps in size with the mean free path l associated with the two thermal energy carriers, namely, electrons, predominantly in metals ($l_e = 10\,\mathrm{nm}$) [23], and phonons, in insulators and semiconductors ($l_{ph} = 10$–$100\,\mathrm{nm}$) [24].

While far field optical methods of thermal conductivity measurement are limited in lateral spatial resolution by diffraction and generally require deposition of Au films on the sample's surface [20–22] as well as contact techniques such as the 3ω method imply deposition of metal contacts on the samples' surface, SThM is a relatively new approach for thermal conductivity measurements allowing the thermal investigation of small size subsurface volumes without any preliminary processing of the sample's surface [25–28]. Using a very localized heat source, SThM appears as a promising method to investigate the thermal properties of the thin films of submicrometric thicknesses used in the designing of more and more integrated devices in microelectronics. Therefore, the SThM technique was used in our study to measure the thermal conductivity of thin meso-PS films.

The principle of the SThM measurement is based on the control of the thermal near field interaction between a small thermal probe and a surface. The technique is similar to atomic force microscopy (AFM) and keeps the probe–sample interatomic force constant and accurately scans the surface when imaging is performed. Its key element is a thermal probe. For fifteen years, various thermal probe prototypes (thermocouple or thermoresistive elements integrated at the apex of AFM probes) [29] have been proposed. We use the thermoresistive wire probe developed by Dinwiddie *et al* in 1994 [30]. This thermal probe consists of a 5 μm diameter and 200 μm length platinum wire bent in the form of a loop. In the used active mode of the probe, the tip acts as a hot anemometer. Sufficient current is passed through the probe to produce self-heating and a feedback system is used to keep the tip temperature constant. When the probe is in contact with a specimen during a scan, the heat flow passing from the tip into the sample is affected by the variation of the local thermal conductivity of the sample subsurface that leads to a modification of the electrical power necessary to maintain the probe temperature constant. The variations of this power are used to obtain the contrast in the thermal image and to study the thermophysical properties of the sample.

The thermal conductivity λ of an optically and thermally thick, isotropic, bulk material can be directly extracted from the device calibration curve obtained with bulk samples of known thermal conductivity and from a simple expression linking the thermal conductivity of the sample with the Joule power relative deviation in the probe deduced from measurements made when the tip contacts samples and when it is free in air and far from any surface [31]. For a sample consisting of a thin film on a substrate, such a simple approach cannot be used, since the response of the probe is now a function of the conductivity of both the film and the substrate. The resolution depth depends also on these two properties [32]. So far, the technique has already been applied to thin films at microscopic scale [25–28] but either the measurements were based on a simplified hypothesis or the films thicknesses were chosen larger than the probe's depth resolution experimentally estimated. In the last case the thin film thermal conductivity can be estimated directly from a SThM calibration with bulk samples of known thermal conductivity. The thermal conductivity of several micrometres thick films cannot be taken to be the same as for the films with submicrometric thickness. Thermal conductivity depends not only on the microstructure of the involved material that often varies with the film thickness but also on the film thickness. As a result of this, the method is limited to the study of films of a few micrometres thickness.

In our recent work [32], we have proposed a new model for the prediction of the SThM measurements in the dc regime and a new method to calibrate the microscope for thermal conductivity measurements on thin films with much better accuracy in comparison with the methods which have been used and reported before. Taking into account the thermal response of the probe and more elaborate descriptions of the thermal interaction of the probe with the sample, this model allowed the performance of the theoretical studies of the SThM response for thin films whatever be their thicknesses. In particular, our results have verified that the SThM sensitivity to the sample thermal conductivity λ_s is significant for the λ_s values which are smaller than a few tens of $\mathrm{W\,m^{-1}\,K^{-1}}$ and therefore it is well adapted in particular for insulator material characterization. It was also shown that the depth resolution of the technique for a given probe would be at most 4 times the range radius of the probe/sample thermal interaction.

For the present work, we apply the new modelling approach for characterization of the effective thermal conductivity of the meso-PS thin films formed on a monocrystalline silicon substrate. Measurements for different film porosities and thicknesses were performed in order to estimate the influence of both layer porosity and thickness on the thermal conductivity of the PS films. Section 2 of this paper gives the description of both the SThM method used and the samples studied. Before the conclusion, the experimental results and their processing are given and discussed in section 3.

2. Measurement technique and samples preparation

2.1. The scanning thermal microscope

Our SThM is the ThermoMicroscope Autoprobe CP Research scanning probe microscope. It is based on an atomic force microscope (AFM) used in contact and constant force modes and equipped with a thermal unit (figure 1). A thermoresistive probe consisting of a 5 μm diameter and 200 μm length platinum wire bent in the form of a loop and acting as a hot wire anemometer replaces the usual AFM SiN_x tip [29]. It is electrically heated and is simultaneously used as a detector and a heat source for the sample. By monitoring the current necessary to keep its temperature constant during a sample scan, the method allows us to map the local thermal conductivity of the surface with a submicrometric lateral resolution [33].

When the heat losses of the probe change, the corresponding change in the heat rate P electrically dissipated in the probe is controlled by measuring the voltage balance in a wheastone bridge. Lefèvre *et al* [31] have proposed a simple expression relating the thermal conductance of bulk samples F to the Joule power relative deviation $(\Delta P/P)$:

$$\Delta P/P = 3GF(8GG_P + 4(2G_P + G)F)^{-1}, \tag{1}$$

where

$$\Delta P/P = (V_{Pc}^2 - V_{Pi}^2)/V_{Pc}^2, \tag{2}$$

in which V_{pi} and V_{pc} are, respectively, the probe voltage for a free tip (in air) and for the tip in contact with the sample, $G_P = 2\lambda_{pt}S/L$ is the thermal conductance of the tip where λ_{Pt} is the platinum/10% rhodium thermal conductivity, S is the probe section and L is the platinum wire length. It is estimated

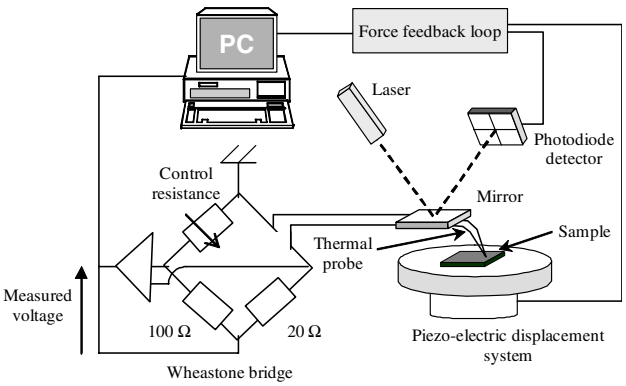

Figure 1. Schematic view of our SThM experimental set-up.

from the dimensional and thermal characteristics of the probe that G is the thermal conductance of the thermal contact.

In the case of a thin film, the substrate influences the measurement as long as the film thickness does not reach the depth resolution of the technique μ. We then extend the model to the configuration of a monolayered sample [34]. In this model, the sample is assumed to be composed of a layer of thickness e located at the surface of a homogeneous semi-infinite solid substrate. The thermal parameters of the sample are characterized by λ_{s1} and λ_{s2}, the thermal conductivity of the film and underlying substrate, respectively. Considering that the sample receives on its surface a heat flow coming from the thermal probe and assuming homogeneous interaction on the whole area of the probe/sample interface ($r \leqslant b$), the sample response is described by the following expression:

$$F = \left(\frac{1}{\pi b^2}\int_0^\infty \mathrm{d}q 2(1+\Re)J_1^2(qb)(\lambda_{s1}q^2(1-\Re))^{-1}\right)^{-1} \tag{3}$$

with

$$\Re = (\lambda_{s1} - \lambda_{s2})\mathrm{e}^{-2qe}/(\lambda_{s1} + \lambda_{s2}). \tag{4}$$

Furthermore, in our model, the thermal conductance of the thermal contact G is given by

$$G = G_g + 2\pi a_c \lambda_{Pt}.\lambda_s/(\lambda_{Pt} + \lambda_s) \tag{5}$$

where G_g is the thermal conductance at the probe/sample interface due to conduction through the air, a_c is the solid–solid contact radius and λ_s is the thermal conductivity of the material which is in direct contact with the probe.

For a given probe, the parameters G_g, a_c and b are unknown. We will see in section 3.1 of this paper that they can be identified from the experimental calibration of the technique with the use of bulk materials of known thermal conductivity. In the case of such materials, $\lambda_{s1} = \lambda_{s2}$ and $R = 0$. So,

$$F = 3\pi^2 b\lambda_s/8. \tag{6}$$

G_g, a_c and b parameters are then determined from the best fitting between the experimental and simulated curves from the combination of equations (1), (2), (5) and (5).

2.2. Fabrication of meso-PS samples

The studied meso-PS layers were obtained by localized electrochemical dissolution [35] of mono-crystalline silicon substrates in electrolyte solutions composed of a mixture of 50% HF acid and absolute ethanol in a ratio of 1 : 1. For fabrication of the samples, (1 0 0)-oriented p+-type (boron doped) Si wafers ($10^{-2}\,\Omega\,$cm) were used. The meso-PS layers are constituted of Si crystallites with sizes of about 10–20 nm. It is well known that the obtained porous material has a strongly anisotropic columnar-like morphology with many lateral ramifications [36].

The electrochemical formation of the PS nanostructures depends on both anodization current and concentration of fluorine ions in the electrolyte solution. If a constant current density is maintained in time, diffusion-induced decreasing of the fluorine ion concentration is responsible for the appearance of strong in-depth morphological non-homogeneity in the porous layers. In order to obtain a more homogeneous

porous layer, we have used a pulsed anodization regime. In this regime, introduction of stop-etch intervals (zero anodization current density periods), restoring composition of the electrolyte solution in depth of the nanoscale pores, ensures in-depth morphological homogeneity of the porous layers. Samples with differing porosities (30%, 54% and 80%) and thicknesses ranging from 38 nm to 7.2 μm were fabricated. Table 1 summarizes the main characteristics of the samples studied.

For each studied porosity, meso-PS films with thicknesses larger than 10 μm were also fabricated and their thermal conductivities were estimated from micro-Raman-spectroscopy measurements using the method reported earlier [4,37]. These thermal conductivity values varying from 1 to 6.5 W m^{-1} K^{-1} are given in table 1. For such relatively low thermal conductivities of a few W m^{-1} K^{-1} [32], the normalized sensitivity of the SThM apparatus to the variation of the effective area size of the probe/sample thermal interaction interface is very high. Therefore, it appeared indispensable to choose samples without strong topographic features to correctly estimate their thermal conductivities by SThM. To study surface topography of the porous samples, an AFM probe was used. Figure 2 gives an example of a topography image obtained in the tapping scanning mode on a meso-PS thin film of porosity of 54%.

Table 1. Characteristics of the studied meso-porous Si/Si films.

Porosity (%)		
30	54	80
Meso-PS film thicknesses (nm)		
1880		5640
1630		4700
1160		3290
690	7200	2000
573	5600	1620
382	4400	1120
286	2800	838
190	1400	559
95	700	279
38	200	112
Thermal conductivity λ_{s1} (W m^{-1} K^{-1})[a]		
6.5	2.6	1.2

[a] Thermal conductivity values were estimated from micro-Raman spectroscopy [4] on meso-PS films with thicknesses >10 μm.

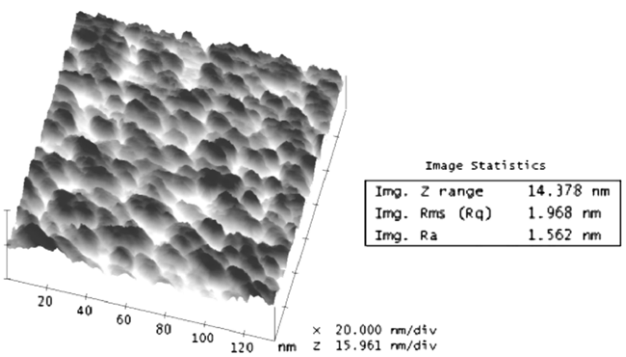

Figure 2. Topography image of a fabricated meso-PS sample with a porosity of 54%.

Low roughness (<4 nm) was observed on all the samples studied. Such a roughness level is favourable for the SThM analysis.

3. SThM measurements

3.1. SThM calibration

Table 2 gives the thermal conductivity of each material used to calibrate the SThM probes used for this study. The samples were well polished to avoid any influence of topography on the thermal signal. Their roughness values measured by AFM are also listed in table 2.

All SThM measurements were carried out with a probe temperature of about 100 °C to avoid the appearance of a water film between the probe and the sample surface which can considerably influence the thermal transfer from the probe to the sample surface [38]. Figure 3 shows the result of the calibration of the probe used for measurements on the samples studied in this work.

The estimated accuracy in the determination of the $\Delta P/P$ ratio from the experimental measurements with the use of (2) is around 5%. Values of $b_{eq} = 0.6\,\mu\text{m} \pm 5\%$, $G_g = 4.7 \times 10^{-6}\text{W K}^{-1} \pm 1\%$ and $a_c = 10$ nm were deduced from the fitting curves computed from a combination of equations (1), (2), (5) and (6).

As can be seen in figure 3, the calibration curve is not linear and thus, a degradation of the measurement sensitivity

Table 2. Thermal conductivity of the calibration standards[a].

Materials[a]	Thermal conductivity, λ_s (W m^{-1} K^{-1})	Roughness (nm)
SiO_2	1.2	3.25
ZnS	1.73	6.27
ZnO	2.5	2.19
CdSe	3.49	0.86
CdTe	6.28	3.7
ZnTe	12.39	5.08
CdS	15.9	1.71
V	31	2.35
Steel40	40	1.49
Ge	58.6	0.604
Dural	147	1.29

[a] Data given by Neyco, the supplier of the samples.

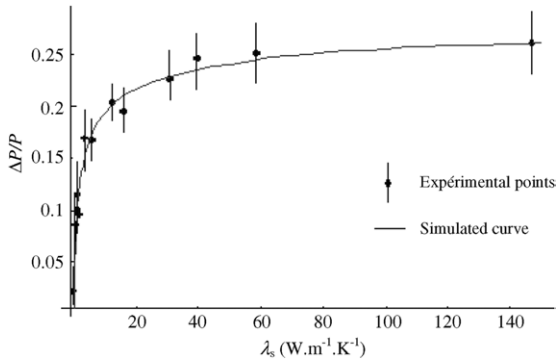

Figure 3. Calibration curves of the SThM for the thermal conductivity measurement.

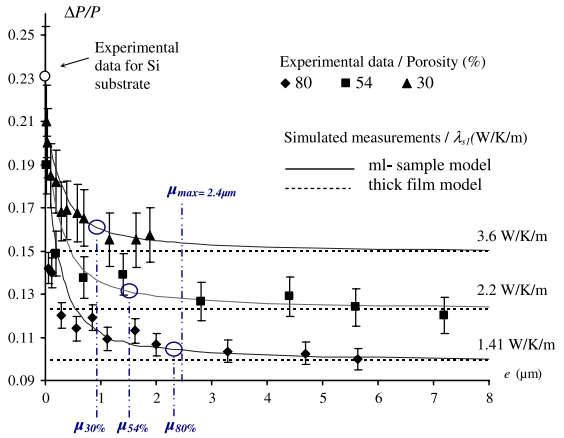

Figure 4. Evolution of the $\Delta P/P$ signal versus the thickness of the thin film of meso-porous silicon for each value of the studied porosity.

(This figure is in colour only in the electronic version)

for materials with thermal conductivities λ_s higher than a few tens of $\mathrm{W\,m^{-1}\,K^{-1}}$ takes place.

3.2. Experimental results for thin meso-PS films and discussion

Measurements on thin meso-PS films were performed with the probe for which the calibration curve is given in figure 3. The experimental conditions for these measurements were the same as those for the probe calibration: measurements in ambient air and a probe's temperature of about 100 °C. Because meso-porous silicon is relatively friable material, all the measurements were done without scan to avoid any probe contamination. The estimated accuracy in the determination of $\Delta P/P$ from these experimental measurements with the use of (2) is also around 5%.

Figure 4 shows the evolution of the measured $\Delta P/P$ ratio versus the thickness of the porous film for each value of the studied porosity. Experimental values are represented by points.

The values of $\Delta P/P$ measured for $e = 0$ correspond well to that of monocrytalline silicon with a thermal conductivity of $147\,\mathrm{W\,m^{-1}\,K^{-1}}$. Solid lines in figure 4 are the theoretical curves calculated from (1) to (5) in which $b_{eq} = 0.6\,\mu\mathrm{m}\pm5\%$, $G_g = 4.7 \times 10^{-6}\,\mathrm{W\,K^{-1}}\pm1\%$ and $a_c = 10\,\mathrm{nm}$ have been used. In our simulations, λ_{s2} is a fixed parameter and it corresponds to the monocrystalline silicon. For each value of the studied porosity, the values of λ_{s1} were obtained from the calibration curve corresponding to the used probe and to the experimental data obtained when the SThM measurements are no more affected by the substrate (thick films). In summary, λ_{s1} values of 3.6 ($\pm10\%$) $\mathrm{W\,m^{-1}\,K^{-1}}$, 2.2 ($\pm7\%$) $\mathrm{W\,m^{-1}\,K^{-1}}$ and 1.41 ($\pm4\%$) $\mathrm{W\,m^{-1}\,K^{-1}}$ were used for porosities of 30%, 54% and 80%, respectively. These estimations are in agreement with those (given in table 2) obtained from micro-Raman spectroscopy measurements performed on meso-PS films of 10 μm thickness. Let us remark that we did not calculate $\Delta P/P$ for the thicknesses lower than 10. $a_c = 100\,\mathrm{nm}$. In this case, the modelling used to describe the thermal conductance of the solid–solid contact is no more valid.

For a given thickness of the porous film, one can see in figure 4 that the lower the $\Delta P/P$ ratio, the higher the porosity of PS. For the studied meso-PS layers, the SThM measurements are really sensitive to the effective thermal conductivity of this anisotropic material. The boundary sides of the silicon nanocrystallites constitute efficient scattering points for phonons and, consequently, it leads to the decrease of the in-plane-thermal conductivity $\lambda_{s1\parallel}$ of the PS layers. In addition, the presence of nano-pores and the phonon confinement effect present in the very small silicon crystallites of diameters 10–20 nm for the studied porous layers (for comparison, $l\mathrm{p} = 40$–$260\,\mathrm{nm}$ for monocrystalline Si) contribute also to the decrease of the effective thermal conductivity of the PS measured with the thermal probe.

Furthermore, we can see that the measurements are all the more sensitive to the variation of the thickness e of PS films than the porosity which is large. This is in good accordance with the results obtained from the theoretical study of SThM sensitivity to the thickness of films given in ref [34]. For each porosity $x\%$ studied, $\mu_{x\%}$ in figure 4 corresponds to the e value for which $(\Delta P/P)_{\mathrm{bulk}x}\% - \beta) - (\Delta P/P)_{\mathrm{ml}x}\% = 0$ where $(\Delta P/P)_{\mathrm{bulk}}$ and $(\Delta P/P)_{\mathrm{ml}}$ were calculated for thick and thin films, respectively, and β is the uncertainty in the measurement of $(\Delta P/P)_{\mathrm{ml}x}\%$. $\mu_{\max}$ was estimated as given in [32]. For a thermal contact radius $b = 600\,\mathrm{nm}$, we verify that the in-depth resolution μ of the thermal probe used depends on the thermal conductivity of the film and is lower than $\mu_{\max} = 4 \cdot b = 2.4\,\mu\mathrm{m}$.

The results in figure 4 show a good agreement between the experimental and the simulated results for the film thicknesses larger than 1 μm whatever be the porosity. However, for smaller thicknesses, simulated values of $\Delta P/P$ over-estimate the SThM signal. To explain this result, we may suggest that the effective thermal conductivity of meso-PS film changes for thicknesses $e < 1\,\mu\mathrm{m}$. For such low thicknesses, the phenomena of constriction at the film/substrate interface, at the level of the interconnections between silicon crystallites and silicon substrate, are manifested in the SThM measurements. This acts as a thermal resistance and lowers the effective thermal conductivity.

We calculated the values of the effective thermal conductivity of meso-PS films from the inversion of our modelling by the Gauss method [39] for the experimental values of $\Delta P/P$ given in figure 4. Figure 5 gives the values obtained for the best accordance between the calculated and experimental values of $\Delta P/P$ for each thickness and porosity studied.

Results in figure 5 seem to show that the effective thermal conductivity of the meso-PS film decreases with the thickness decreasing (starting from the value of 1 μm), whatever be the porosity of the film. This behaviour of thermal conductivity has been already found in other materials, for example: SiO_2 [25]. A modelling is required to extract the film thermal conductivity from the apparent conductivity λ_{s1} measured by SThM. Assuming that the in-plane thermal conductivity of the meso-PS film, $\lambda_{\mathrm{mPS}\parallel}$, is negligible compared with the transverse thermal conductivity, $\lambda_{\mathrm{mPS}\top}$, we tested the one-dimensional terminology introduced by Lambropoulos [39] to process our data of λ_{s1}. We then plotted e/λ_{s1} as a function of the film thickness e. Figure 6 represents the experimental

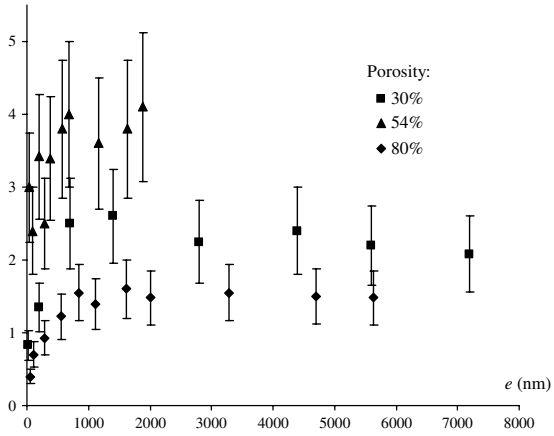

Figure 5. Evolution of the effective thermal conductivity of the meso-PS film–interface system versus the thickness of film for each porosity studied.

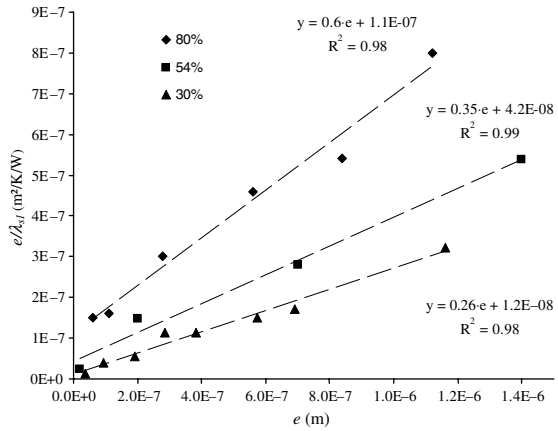

Figure 6. Evolution of e/λ_{s1} ratio versus the thickness e of PS films for each porosity studied. The dashed lines are the best fits of the data obtained with a least square fit method. The equation of the lines are $e/\lambda_{s1} = (0.6 \cdot e + 1 \times 10^{-7})$, $e/\lambda_{s1} = (0.35 \cdot e + 4.2 \times 10^{-7})$ and $e/\lambda_{s1} = (0.26 \cdot e + 1.2 \times 10^{-8})$ for the porosities of 80%, 54%, 30%, respectively.

variation of e/λ_{s1} as a function of e. It shows that this variation is linear whatever be the porosity of meso-PS. λ_{s1} can be then expressed as a function of an intrinsic film thermal conductivity λ_{mPS} and an interfacial thermal resistance R_{int} through the relationship [25]

$$\frac{e}{\lambda_{s1}} = \frac{e}{\lambda_{mPS}} + R_{int}. \tag{7}$$

Equation (7) describes that the total resistance of the assembly film/interface is the sum of the resistance of the film and the resistance of the film/substrate interface. It is a 1D representation of thermal conduction in films. Using (7) and figure 6, λ_{mPS} and R_i can be determined. Table 3 gives the values of theses parameters for each of the studied porosities.

The values of thermal conductivity obtained for meso-PS films of submicrometric thickness are in accordance with the values measured by SThM for films of common materials (films of several micrometers) and values estimated from Raman spectroscopy measurements (films of several tens of micrometers) (see figure 7).

Table 3. Thermal conductivity and interfacial thermal resistance for meso-PS films of submicrometric thickness versus porosity.

Porosity (%)	λ_{mPS} (W m^{-1} K^{-1})	R_i (m^2 K^{-1} W^{-1})
30	3.8	1.2×10^{-8}
54	2.8	4.2×10^{-7}
80	1.7	1×10^{-7}

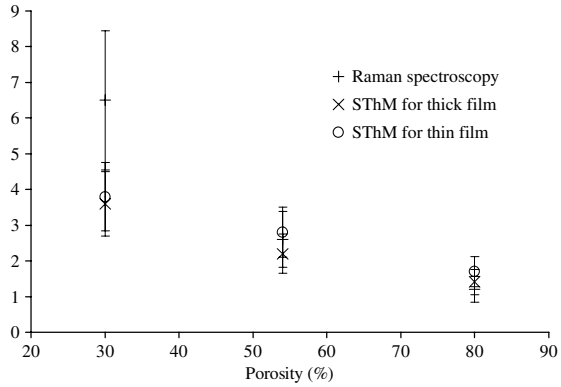

Figure 7. Thermal conductivity of meso-PS layers as a function of porosity obtained by Raman spectroscopy and SThM measurements on thick and thin meso-porous samples.

These results tend to show that the higher the porosity, the larger the interfacial thermal resistance R_{int}. This means that the effect of cumulated constrictions at the Si crystallites–bulk Si substrate interface is more important for PS films with higher porosity.

4. Conclusions and perspectives

A SThM equipped with a micrometric thermal wire probe was used to determine the thermal conductivity of homogeneous in-depth thin meso-porous silicon films in the thickness range from 100 nm to 8 μm. The measurements were performed on some reference materials to determine the parameters defining the calibration curve of the probe, namely, an effective thermal contact and solid–solid contact radii and thermal conductance of the probe/sample interaction. Further, we used these parameters in a modelling that we described earlier [32] to estimate the effective thermal conductivity of meso-PS films. The effective thermal conductivity values decrease with increasing porosity whatever be the film thickness. The thermal conductivity values measured for film thicknesses larger than 1 μm are in good accordance with those measured by micro-Raman-spectroscopy on bulk (thick) meso-PS samples. SThM is then sensitive to the intrinsic thermal conductivity of the studied materials. For the submicrometric thicknesses (<1 μm), the SThM is in addition sensitive to the presence of the interfacial thermal resistance between the film and the substrate. As a result, the measured effective thermal conductivity decreases with decreasing film thickness. From these measurements, we were able to extract an intrinsic thermal conductivity of the layer as well as a thermal resistance at the interface. The obtained values of thermal conductivity are equal to those measured for micrometric thicknesses. From the apparatus point of view, this work shows that in our used experimental conditions (used probe, dc regime, temperature

of probe about 100 °C and measurements in ambient), the SThM investigation depth is around 1 μm. This result validates the data calculated and reported previously [32].

Furthermore, different temperature-modulation regimes for the concerned SThM wire probe were or are actually developed to improve the sensitivity of SThM, to be able to control the volume of matter probed by adjusting the modulation frequency of the probe temperature and/or by modulating the force applied to the sample (see [29, 40, 41]). Works of Fiege *et al* [40] have notably shown that probe-to-probe variations in contact area could be eliminated by means of reference measurements on standard samples of known thermal conductivity. We plan to study and apply them for the thermal characterization of insulator thin films.

Acknowledgments

This work was supported by the National Institute of Applied Sciences of Lyon. The authors thank S Lallich for his thermal conductivity measurements on these materials with the micro-Raman-spectroscopy method.

References

[1] Delan A, Rennau M, Schulz S E and Gessner T 2003 *Microelectronic Eng.* **70** 280–84
[2] Lysenko V, Périchon S, Remaki B and Barbier D 2002 *Sensors Actuators* A **99** 13–24
[3] Perichon S 2001 *PhD Thesis* Institut National des Sciences Appliquées de Lyon, France
[4] Lysenko V, Perichon S, Remaki B, Barbier D and Champagnon B 1999 *J. Appl. Phys.* **86** 6841–6
[5] Drost A, Steiner P, Moser H and Lang W 1995 *Sensors and Materials* **7** 111–20
[6] Gesele G, Linsmeier J, Drach V, Fricke J, Arens-Fischer R 1997 *J. Phys. D: Appl. Phys.* **30** 2911–16
[7] Benedetto G, Boarino L and Spagnolo R 1997 *Appl. Phys.* A **64** 155–9
[8] Bernini U, Maddalena P, Massera E and Ramaglia 1999 *J. Opt. A: Pure Appl. Opt.* **1** 210–13
[9] Shen Q and Toyoda T 2003 *Rev. Sci. Intrum.* **74** 601–3
[10] Bernini U, Lettieri S, Maddalena P, Vitiello R and Di Francia G 2001 *J. Phys.: Condens. Matter* **13** 1141–50
[11] Bernini U, Lettieri S, Massera E and Rucco P A 2003 *Opt. Lasers Eng.* **39** 127–40
[12] Cahill G, Bullen A and Lee S M 2000 *High Temp.–High Pressures* **32** 135–42
[13] Orain S, Schudeller Y and Brousse T 2000 *Int. J. Therm. Sci.* **39** 537–43
[14] Asheghi M, Kurabayashi K, Kasnavi R and Goodson K E 2002 *J. Appl. Phys.* **91** 5079–88
[15] Chen G, Shakouri 2002 *J. Heat Transfer* **124** 242–52
[16] Bhusari D M, Teng C W, Chen K H, Wei S L and Chen L C 1997 *Rev. Sci. Instrum.* **68** 4180–3
[17] Langer G, Hartmann J and Reichling M 1997 *Rev. Sci. Instrum.* **68** 1510–13
[18] Li B, Roger J P, Pottier L and Fournier D 1999 *J. Appl. Phys.* **86** 5314–16
[19] Dilhaire S, Grauby S, Clayes W and Batsale J Ch 2004 *Microelectron. J.* **35** 811–16
[20] Kusiak A, Battaglia J L, Gomez S, Manaud J P and Lepetitcorps Y 2006 *Eur. Phys. J.: Appl. Phys.* **35** 17–27
[21] Schwab K, Henriksen E A Worlock J M and Roukes M L 2000 *Nature (London)* **404** 974–7
[22] Chen G 1997 *J. Heat Transfer* **119** 220–9
Chen G 1998 *Phys. Rev.* B **57** 14858–973
[23] Ruiz F, Sun W D, Pollak F H and Venkatraman C 1998 *Appl. Phys. Lett.* **73** 1802–4
[24] Gorbunov V V, Fuchigami N , Hazel J L and Tsukruk V V 1999 *Langmuir* **15** 8340–3
[25] Callard S, Tallarida G, Borghesi A and Zanotti L 1999 *J. Non-Cryst. Solids* **245** 203–9
[26] Volz S, Feng X, Fuentes C, Guérin P and Jaouen M 2002 *Int. J. Thermophys.* **23** 1645–57
[27] Meinders E R 2001 *J. Mater. Res*. **16** 2530–42
[28] Asnin V M, Pollak F H, Ramer J C, Schurman M J and Ferguson I 1999 *Appl. Phys. Lett.* **75** 1240–2
[29] Majumdar A 1999 *Annu. Rev. Mater. Sci.* **29** 505–85
[30] Dinwiddie R B, Pylkki R J and West P E 1994 *Thermal Cond.* **22** 668–77
[31] Lefèvre S, Volz S, Saulnier J B, Fuentes C and Trannoy N 2003 *Rev. Sci. Instrum.* **74** 2418–23
[32] David L, Gomès S and Raynaud M 2007 *J. Phys. D: Appl. Phys.* **40** 4337–46
[33] Pollock H M, Hammiche A 2001 *J. Phys. D: Appl. Phys.* **34** R23–53
[34] David L 2006 *Thesis* Institut National des Sciences Appliquées de Lyon, France
[35] Betzner T M, Dorty J R, Hamad A M A, Henderson H T and Berger F G 1996 *J. Micromech. Microeng.* **6** 217–27
[36] Smith R L and Collins S D 1992 *J. Appl. Phys.* **71–8** R1–R22
[37] Perichon S, Lysenko V, Roussel Ph, Remaki B, Champagnon B, Barbier D and Pinard P 2000 *Sensors Actuators* **85** 335–9
[38] Gomès S, Trannoy N and Grossel Ph 1999 *Meas. Sci. Technol.* **10** 805–11
[39] Lambropoulos J C, Jolly M R, Amsden C A, Gilman S E, Sinicropi M J, Diakomihalis D and Jacobs S D 1989 *J. Appl. Phys.* **66** 4230–42
[40] Fiege G B M, Altes A, Heiderhoff R and Balk L J 1999 *J. Phys. D: Appl. Phys.* **32** L13–L17
[41] Lefèvre S 2004 *Thesis* University of Poitiers, France